NCKU-HEP-98-14
NCTU-HEP-9806

Perturbative QCD study of the $B \to K^*\gamma$ decay

Hsiang-nan Li[a] and Guey-Lin Lin[b]
[a]Department of Physics, National Cheng-Kung University, Tainan 701, Taiwan, Republic of China
[b]Institute of Physics, National Chiao-Tung University, Hsinchu 300, Taiwan, Republic of China

Abstract

We apply the perturbative QCD factorization theorem developed recently for nonleptonic heavy meson decays to the radiative decay $B \to K^*\gamma$. In this formalism the evolution of the Wilson coefficients from the W boson mass down to the characteristic scale of the decay process is governed by the effective weak Hamiltonian. The evolution from the characteristic scale to a lower hadronic scale is formulated by the Sudakov resummation. Besides computing the dominant contribution arising from the magnetic-penguin operator O_7, we also calculate the contributions of four-quark operators. By fitting our prediction for the branching ratio of the $B \to K^*\gamma$ decay to the CLEO data, we determine the B meson wave function, that possesses a sharp peak at a low momentum fraction.

PACS numbers: 13.25.Hw, 11.10.Hi, 12.38.Bx

I. INTRODUCTION

The observation of the decay $B \to K^*\gamma$ five years ago [1] opened a new era for particle physics, since the penguin structure of the electroweak theory was probed for the first time. Soon after this observation, the inclusive $B \to X_s\gamma$ decay [2] was also established. The updated branching ratios for both decays are $(4.2 \pm 0.8 \pm 0.6) \times 10^{-5}$ [3] and $(3.14 \pm 0.48) \times 10^{-4}$ [4,5], respectively. In recent literatures, the inclusive decay $B \to X_s\gamma$ receives more attentions than the exclusive mode $B \to K^*\gamma$. The branching ratio and the photon energy spectrum of the $B \to X_s\gamma$ decay have been used to constrain the parameter-space of the new physics beyond the standard model. The preference of studying the inclusive mode is clear in that its hadronic dynamics is much easier to handle as compared to the exclusive mode. It has been shown that, to the leading order in $1/M_b$, M_b being the b quark mass, the branching ratio $\mathcal{B}(B \to X_s\gamma)$ is given by the branching ratio $\mathcal{B}(b \to s\gamma)$ of the corresponding quark-level process. Furthermore, the sub-leading $1/M_b$-corrections can be parametrized systematically using the heavy quark effective theory [6].

The hadronic dynamics of the exclusive decay $B \to K^*\gamma$ is much more complicated. Specifically, one has to deal with the soft dynamics involved in the B and K^* mesons. Since the final states are light compared to the decaying B meson, one anticipates that perturbative QCD (PQCD) is applicable to this process because of the large energy release. In fact, the PQCD formalism based upon factorization theorems, which incorporates the Sudakov resummation of soft-gluon effects, has been developed for sometime [7–9], and applied to semileptonic [7,8], inclusive-radiative [9] and nonleptonic B meson decays [10]. This approach is so far rather successful. In this article, we shall extend this formalism to penguin-induced exclusive processes, such as the $B \to K^*\gamma$ decay. The satisfactory result with repect to this complicated process, as presented later, provides further confidence on the validity of the PQCD approach to B meson decays.

According to the PQCD factorization theorem, the branching ratio of a heavy meson decay is expressed as the convolution of a hard subamplitude with meson wave functions. The former, with at least one hard gluon attaching to the spectator quark, is calculable in the usual perturbation theory, while the latter must be extracted from the experimental data or derived by nonperturbative methods, such as QCD sum rules. Since the K^* meson wave function has been known from the sum rule analyses [11,12], the $B \to K^*\gamma$ decay is an ideal process from which the unknown B meson wave function can be determined. With the B meson wave function obtained here, we are able to make predictions for other B meson decay modes, especially for the charmless decays. We shall show that by fitting our prediction for the branching ratio $\mathcal{B}(B \to K^*\gamma)$ to the CLEO data, a B meson wave function with a sharp peak at the low momentum fraction is obtained.

Comparing our work to others, we remark that most of the previous studies on this decay focus only on the contribution of the magnetic-penguin operator O_7, and their approaches are based upon quark models. To ensure that other contributions are indeed negligible, we also calculate the contribution by the current-current operator O_2, which arises through the four-point $b \to sg^*\gamma$ coupling with the off-shell gluon reabsorbed by a spectator quark. Although such a contribution has been calculated before [13], it is however obtained in a naive PQCD framework which does not include the Sudakov resummation and the renormalization-group (RG) analysis [13]. As a result, the predictions of Ref. [13] are sensitive to the choice of

the renormalization scale μ. In our more completed approach, the sensitivity to μ can be avoided. We find that, due to certain cancellations, the contribution by O_2 turns out to be rather small.

We also like to comment on a different viewpoint based on the overlap integral of meson wave functions [14], which showed that the diagrams without any hard gluon dominate over those we will be considering here. We shall argue that the observation in [14] is due to an underestimation on the value of the strong coupling constant and a choice of a flat B meson wave function. If evaluating the coupling constant at the characteristic momentum flow involved in the decay process [13], and employing a sharper B meson wave function, these higher-order contributions may become comparable to the leading-order ones. Hence, the approach in [14] does not seem to be self-consistent. In our approach, the diagrams without hard gluons do not contribute under our parametrization of parton momenta. Therefore, the diagrams with a hard gluon attaching to a spectator are leading in our analysis.

This article is organized as follows: In Sect. II, we write down the effective Hamiltonian for the $B \to K^*\gamma$ decay. In particular, the current-current operator O_2 and the magnetic-penguin operators O_7 are identified as major sources of the contribution. We then calculate the O_2-induced $b \to sg^*\gamma$ vertex, keeping the gluon line off-shell. In Sect. III, we derive the factorization formulas for the $B \to K^*\gamma$ decay, which include contributions from the various operators. The numerical result is presented in Sect. IV, where the contribution of each operator is compared. Sect. V is the conclusion.

II. EFFECTIVE HAMILTONIAN

The effective Hamiltonian for the flavor-changing $b \to s$ transition is now standard, which is given by [15,16]

$$H_{\rm eff}(b \to s\gamma) = -\frac{G_F}{\sqrt{2}} V_{ts}^* V_{tb} \sum_{i=1}^{8} C_i(\mu) O_i(\mu) \tag{1}$$

with

$$\begin{aligned}
O_1 &= (\bar{s}_i c_j)_{V-A} (\bar{c}_j b_i)_{V-A} \\
O_2 &= (\bar{s}_i c_i)_{V-A} (\bar{c}_j b_j)_{V-A} \\
O_3 &= (\bar{s}_i b_i)_{V-A} \sum_q (\bar{q}_j q_j)_{V-A} \\
O_4 &= (\bar{s}_i b_j)_{V-A} \sum_q (\bar{q}_j q_i)_{V-A} \\
O_5 &= (\bar{s}_i b_i)_{V-A} \sum_q (\bar{q}_j q_j)_{V+A} \\
O_6 &= (\bar{s}_i b_j)_{V-A} \sum_q (\bar{q}_j q_i)_{V+A} \\
O_7 &= \frac{e}{4\pi^2} \bar{s}_i \sigma^{\mu\nu} (m_s P_L + m_b P_R) b_i F_{\mu\nu} \\
O_8 &= \frac{g}{4\pi^2} \bar{s}_i \sigma^{\mu\nu} (m_s P_L + m_b P_R) T^a_{ij} b_j G^a_{\mu\nu},
\end{aligned} \tag{2}$$

i, j being the color indices. In the PQCD picture, the lowest-order diagrams for the $B \to K^*\gamma$ decay arising from operators O_2, O_7 and O_8 are depicted in Figs. 1-3. It is not hard to see that contributions other than the above are negligible. For example, contributions depicted in Fig. 4 are very suppressed, although they are of the same order, $O(eG_F\alpha_s)$ [17], as those of Figs. 1-3. We draw this conclusion from a previous experience with $B \to D^*\gamma$. Indeed, from a diagram similar to Fig. 4 (with s replaced by c, and the $\bar{q}$ on both sides replaced by $\bar{d}$ and $\bar{u}$, respectively), one has obtained $\mathcal{B}(B \to D^*\gamma) = 10^{-6}$ [18]. Since $f_{K^*} \approx f_{D^*}$, and $V_{tb}V_{ts}$ is comparable to $V_{cb}V_{ud}$, it is clear that the diagram in Fig. 4 gives $\mathcal{B}(B \to K^*\gamma) \approx 10^{-6} \times C^2_{3(4,5,6)} \approx 10^{-9} - 10^{-10}$, and is thus negligible. There is still one more type of contributions of the same order as shown in Fig. 5. By an explicit calculation, one can show that such contributions merely give corrections to the Wilson coefficients C_3-C_6 occuring in Fig. 4. Since the matrix elements of Fig. 4 and Fig. 5 have identical tensor structures, the branching ratio contributed by the latter figure behaves like $10^{-6} \times C_2^2 \times (\frac{\alpha_s}{\pi})^2 \approx 10^{-9}$, which is also negligible. Finally, in Sect. IV, we shall see that the contribution by O_8 is negligible as well.

Before implementing the PQCD formalism to evaluate the contributions of Figs. 1-3, we compute the four-point $b \to sg^*\gamma$ vertex. Our calculation essentially generalizes the work by Liu and Yao [19] to the off-shell gluon case [20]. We first perform a Fierz transformation on O_2, *i.e.*,

$$O_2 \equiv (\bar{s}_i c_i)_{V-A}(\bar{c}_j b_j)_{V-A} = (\bar{s}_i b_j)_{V-A}(\bar{c}_j c_i)_{V-A}. \tag{3}$$

The $b(p) \to s(p')\gamma(k_1)g^*(k_2)$ vertex is expressed as

$$I^{a\nu} = C_2 V_{ts}^* V_{tb} \bar{u}(p')\frac{1}{2}\gamma^\rho(1-\gamma_5)T^a u(p) I_{\mu\nu\rho}\epsilon^\mu(k_1), \tag{4}$$

with the structure-tensor

$$\begin{aligned} I_{\mu\nu\rho} = {} & A_1\epsilon_{\mu\nu\rho\sigma}k_1^\sigma + A_2\epsilon_{\mu\nu\rho\sigma}k_2^\sigma + A_3\epsilon_{\mu\rho\sigma\tau}k_1^\sigma k_2^\tau k_{1\nu} \\ & + A_4\epsilon_{\nu\rho\sigma\tau}k_1^\sigma k_2^\tau k_{2\mu} + A_5\epsilon_{\mu\rho\sigma\tau}k_1^\sigma k_2^\tau k_{2\nu} + A_6\epsilon_{\nu\rho\sigma\tau}k_1^\sigma k_2^\tau k_{1\mu}. \end{aligned} \tag{5}$$

Clearly, the form factor A_6 can be discarded because of $k_1 \cdot \epsilon(k_1) = 0$. From the requirement of gauge invariance, *i.e.*, $k_1^\mu I_{\mu\nu\rho} = 0$ and $k_2^\nu I_{\mu\nu\rho} = 0$, we have

$$\begin{aligned} A_2 + A_4 k_1 \cdot k_2 &= 0 \\ A_1 + A_3 k_1 \cdot k_2 + A_5 k_2^2 &= 0. \end{aligned} \tag{6}$$

The invariance of $I_{\mu\nu\rho}$ under the interchanges $k_1 \leftrightarrow k_2$ and $\mu \leftrightarrow \nu$ further require $A_3 = -A_4$. With the above relations, $I_{\mu\nu\rho}$ is simplified into

$$\begin{aligned} I_{\mu\nu\rho} = {} & A_4\left[k_1 \cdot k_2 \epsilon_{\mu\nu\rho\sigma}(k_1-k_2)^\sigma + \epsilon_{\nu\rho\sigma\tau}k_1^\sigma k_2^\tau k_{2\mu} - \epsilon_{\mu\rho\sigma\tau}k_1^\sigma k_2^\tau k_{1\nu}\right] \\ & + A_5\left(\epsilon_{\mu\rho\sigma\tau}k_1^\sigma k_2^\tau k_{2\nu} - k_2^2\epsilon_{\mu\nu\rho\sigma}k_1^\sigma\right), \end{aligned} \tag{7}$$

with

$$A_4 = \frac{2\sqrt{2}}{3\pi^2} e g_s G_F I_{11}(M_c^2)\,, \tag{8}$$

$$A_5 = -\frac{2\sqrt{2}}{3\pi^2} e g_s G_F \left[I_{10}(M_c^2) - I_{20}(M_c^2)\right]\,, \tag{9}$$

and

$$I_{ab}(m^2) = \int_0^1 dx \int_0^{1-x} dy \frac{x^a y^b}{x(1-x)k_2^2 + 2xyk_1\cdot k_2 - m^2 + i\varepsilon}. \tag{10}$$

Carrying out the Feynman-parameter integrations, we obtain

$$\begin{aligned} I_{11}(m^2) = & \left[\frac{1}{2Q^2} + \int_0^1 dx \frac{m^2 - x(1-x)k_2^2}{xQ^4} \ln\left|\frac{m^2 - x(1-x)(k_2^2+Q^2)}{m^2 - x(1-x)k_2^2}\right|\right. \\ & \left. - i\pi\Theta(Q^2 + k_2^2 - 4m^2)\left(\frac{m^2}{Q^4}\ln\frac{1+\beta}{1-\beta} - \frac{\beta k_2^2}{2Q^4}\right)\right], \end{aligned} \tag{11}$$

$$\begin{aligned} I_{10}(m^2) - I_{20}(m^2) = & \left[\int_0^1 dx \frac{1-x}{Q^2} \ln\left|\frac{m^2 - x(1-x)(k_2^2+Q^2)}{m^2 - x(1-x)k_2^2}\right|\right. \\ & \left. - i\pi\Theta(Q^2 + k_2^2 - 4m^2)\frac{\beta}{2Q^2}\right], \end{aligned} \tag{12}$$

with $Q^2 = 2k_1\cdot k_2$, and $\beta = \sqrt{1 - 4m^2/(k_2^2+Q^2)}$. As a side remark, we note that both $I_{11}(m^2)$ and $I_{10}(m^2) - I_{20}(m^2)$ have smooth limits as $m^2 \to 0$. Hence, we can safely neglect the contributions of O_4 and O_6 to the $b \to sg^*\gamma$ vertex, since their Wilson coefficients, C_4 and C_6, are much smaller than C_2.

Having determined the $b \to sg^*\gamma$ vertex, we attach the off-shell gluon line to the spectator quark to form the $B \to K^*\gamma$ amplitude as shown in Fig. 1. As mentioned, this amplitude is of the order $e\alpha_s G_F$, the same as the amplitudes induced by O_7 and O_8 depicted in Figs. 2 and 3, respectively. In the next section, we shall compute the contribution of each operator to the $B \to K^*\gamma$ decay using the PQCD factorization theorem.

III. FACTORIZATION FORMULAS

In this section we first review the PQCD factorization theorem developed for nonleptonic heavy meson decays [10], and then extend it to the $B \to K^*\gamma$ decay. Nonleptonic heavy meson decays involve three scales: the W boson mass M_W, at which the matching conditions of the effective Hamiltonian to the original Hamiltonian are defined, the typical scale t of a hard subamplitude, which reflects the dynamics of heavy meson decays, and the factorization scale $1/b$, with b the conjugate variable of parton transverse momenta. The dynamics below $1/b$ is regarded as being completely nonperturbative, and parametrized into a meson wave fucntion $\phi(x)$, x being the momentum fraction. Above the scale $1/b$, PQCD is reliable and radiative corrections produce two types of large logarithms: $\ln(M_W/t)$ and $\ln(tb)$. The former are summed by RG equations to give the evolution from M_W down to t described by the Wilson coefficients $c(t)$. While the latter are summed to give the evolution from t to $1/b$.

There exist also double logarithms $\ln^2(Pb)$ from the overlap of collinear and soft divergences, P being the dominant light-cone component of a meson momentum. The resummation of these double logarithms leads to a Sudakov form factor $\exp[-s(P,b)]$, which suppresses the long-distance contributions in the large b region, and vanishes as $b = 1/\Lambda$, $\Lambda \equiv \Lambda_{\rm QCD}$ being the QCD scale. This factor improves the applicability of PQCD around

the energy scale of few GeV. The b quark mass scale is located in the range of applicability. This is the motivation we develop the PQCD formalism for heavy hadron decays. For the detailed derivation of the relevant Sudakov form factors, please refer to [7,8].

With all the large logarithms organized, the remaining finite contributions are absorbed into a hard b quark decay subamplitude $H(t)$. Because of Sudakov suppression, the perturbative expansion of H in the coupling constant α_s makes sense. Therefore, a three-scale factorization formula is given by the typical expression,

$$c(t) \otimes H(t) \otimes \phi(x) \otimes \exp\left[-s(P,b) - 2\int_{1/b}^{t} \frac{d\bar{\mu}}{\bar{\mu}} \gamma_q(\alpha_s(\bar{\mu}))\right], \tag{13}$$

where the exponential containing the quark anomalous dimension $\gamma_q = -\alpha_s/\pi$ describes the evolution from t to $1/b$ mentioned above. The explicit expression of the exponent s is can be found in [10]. Since logarithmic corrections have been summed by RG equations, the above factorization formula does not depend on the renormalization scale μ [10]. Our formalism then avoids the sensitivity to μ that appears in [13].

We now apply the three-scale factorization theorem to the radiative decay $B \to K^*\gamma$, whose effective Hamiltonian has been given in the previous section. As stated before, only the operators O_2, O_7 and O_8 are crucial, to which the corresponding diagrams and hard subamplitudes are shown in Figs. 1-3 and Table I, respectively. We write the momenta of B and K^* mesons in light-cone coodinates as $P_B = (M_B/\sqrt{2})(1,1,\mathbf{0}_T)$ and $P_K = (M_B/\sqrt{2})(1,r^2,\mathbf{0}_T)$, respectively, with $r = M_{K^*}/M_B$. The B meson is at rest with the above choice of momenta. We further parametrize the momenta of the light valence quarks in the B and K^* mesons as k_B and k_K, respectively. k_B has a minus component k_B^-, giving the momentum fraction $x_B = k_B^-/P_B^-$, and small transverse components $\mathbf{k}_{BT}$. k_K has a large plus component k_K^+, giving $x_K = k_K^+/P_K^+$, and small $\mathbf{k}_{KT}$. The photon momentum is then $P_\gamma = P_B - P_K$, whose nonvanishing component is only P_γ^-.

The $B \to K^*\gamma$ decay amplitude can be decomposed as

$$M = \epsilon_\gamma^* \cdot \epsilon_{K^*}^* M^S + i\epsilon_{\mu\rho+-}\epsilon_\gamma^{*\mu}\epsilon_{K^*}^{*\rho} M^P \ , \tag{14}$$

with ϵ_γ and ϵ_{K^*} the polarization vectors of the photon and of the K^* meson, respectively. Note that we have neglected the structure $(P_\gamma \cdot \epsilon_{K^*}^*)(P_K \cdot \epsilon_\gamma^*)/(P_\gamma \cdot P_K)$ which should come together with $\epsilon_\gamma^* \cdot \epsilon_{K^*}^*$. This is due to our choice of the frame which gives $P_K \cdot \epsilon_\gamma^* = 0$. From Eq. (14), it is obvious that only the K^* mesons with transverse polarizations are produced in the decay.

The total rate of the $B \to K^*\gamma$ decay is given by

$$\Gamma = \frac{1-r^2}{8\pi M_B}(|M^S|^2 + |M^P|^2) \ . \tag{15}$$

We can further decompose M^S and M^P as

$$M^i = M_2^i + M_7^i + M_8^i \ , \tag{16}$$

where $i = S$ or P, and the terms on the right-hand side represent contributions from operators O_2, O_7, and O_8, respectively.

In the following, we write the factorization formulas for M_l^i in terms of the overall factor

$$\Gamma^{(0)} = \frac{G_F}{\sqrt{2}} \frac{e}{\pi} V_{ts}^* V_{tb} C_F M_B^5 \ . \tag{17}$$

The amplitudes contributed by O_2 is written as

$$\begin{aligned} M_2^S = \Gamma^{(0)} \frac{4}{3} \int_0^1 dx \int_0^{1-x} dy \int_0^1 dx_B dx_K \int_0^{1/\Lambda} b db \phi_B(x_B) \phi_{K^*}(x_K) \\ \times \alpha_s(t_2) c_2(t_2) \exp[-S(x_B, x_K, t_2, b, b)] \\ \times [(1 - r^2 + 2r x_K + 2x_B) y - (r x_K + 3x_B)(1 - x)] \\ \times \frac{(1-r)(1-r^2) x_K x}{xy(1-r^2) x_K M_B^2 - M_c^2} H_2(Ab, \sqrt{|B_2^2|} b) \ , \end{aligned} \tag{18}$$

$$\begin{aligned} M_2^P = \Gamma^{(0)} \frac{4}{3} \int_0^1 dx \int_0^{1-x} dy \int_0^1 dx_B dx_K \int_0^{1/\Lambda} b db \phi_B(x_B) \phi_{K^*}(x_K) \\ \times \alpha_s(t_2) c_2(t_2) \exp[-S(x_B, x_K, t_2, b, b)] \\ \times \Big[\Big((1-r)(1-r^2) + 2r^2 x_K + 2x_B \Big) y \\ - (r(1+r) x_K + (3-r) x_B)(1-x) \Big] \\ \times \frac{(1-r^2) x_K x}{xy(1-r^2) x_K M_B^2 - M_c^2} H_2(Ab, \sqrt{|B_2^2|} b) \ , \end{aligned} \tag{19}$$

with

$$\begin{aligned} A^2 &= x_K x_B M_B^2 \ , \\ B_2^2 &= x_K x_B M_B^2 - \frac{y}{1-x} (1-r^2) x_K M_B^2 + \frac{M_c^2}{x(1-x)} \ , \\ t_2 &= \max(A, \sqrt{|B_2^2|}, 1/b) \ . \end{aligned} \tag{20}$$

To arrive at the above expressions, we have employed Eq. (10) for the charm loop integral, instead of Eqs. (11) and (12). The variable b_B (b_K), conjugate to the parton transverse momentum k_{BT} (k_{KT}), represents the transverse extent of the B (K^*) meson; t_2 is the characteristic scale of the hard subamplitude

$$\begin{aligned} H_2(Ab, \sqrt{|B_2^2|} b) &= K_0(Ab) - K_0(\sqrt{|B_2^2|} b) \ , \quad B_2^2 > 0 \ , \\ &= K_0(Ab) - i \frac{\pi}{2} H_0^{(1)}(\sqrt{|B_2^2|} b) \ , \quad B_2^2 < 0 \ , \end{aligned} \tag{21}$$

which comes from the Fourier transform of the corresponding expressions in Table I to the b space. Note that, for simplicity in the notation, we have used H_2 to denote hard subamplitudes in both M_2^S and M_2^P. In Table I, these two amplitudes are distinguished.

There are two diagrams, Figs. 2(a) and 2(b), associated with the operator O_7, where the hard gluon connects both quarks of the B meson or those of the K^* meson. The amplitudes from the two diagrams are

$$M_7^S = -M_7^P = \Gamma^{(0)} 2 \int_0^1 dx_B dx_K \int_0^{1/\Lambda} b_B db_B b_K db_K \phi_B(x_B)\phi_{K^*}(x_K)(1-r^2)$$
$$\times \left[r H_7^{(a)}(Ab_K, \sqrt{|B_7^2|}b_B, \sqrt{|B_7^2|}b_K) F_7(t_{7a}) \right.$$
$$\left. + [1 + r + (1-2r)x_K] H_7^{(b)}(Ab_B, C_7 b_B, C_7 b_K) F_7(t_{7b}) \right] , \tag{22}$$

with

$$B_7^2 = (x_B - r^2)M_B^2 , \quad C_7^2 = x_K M_B^2$$
$$t_{7a} = \max(A, \sqrt{|B_7^2|}, 1/b_B, 1/b_K) ,$$
$$t_{7b} = \max(A, C_7, 1/b_B, 1/b_K) , \tag{23}$$

where the function F_7 denotes the product

$$F_7(t) = \alpha_s(t) c_7(t) \exp[-S(x_B, x_K, t, b_B, b_K)] . \tag{24}$$

The hard functions

$$H_7^{(a)}(Ab_K, \sqrt{|B_7^2|}b_B, \sqrt{|B_7^2|}b_K) =$$
$$K_0(Ab_K) h(\sqrt{|B_7^2|}b_B, \sqrt{|B_7^2|}b_K) , \quad B_7^2 > 0 ,$$
$$K_0(Ab_K) h'(\sqrt{|B_7^2|}b_B, \sqrt{|B_7^2|}b_K) , \quad B_7^2 < 0 , \tag{25}$$

with

$$h = \theta(b_B - b_K) K_0(\sqrt{|B_7^2|}b_B) I_0(\sqrt{|B_7^2|}b_K) + (b_B \leftrightarrow b_K) ,$$
$$h' = i\frac{\pi}{2} \left[\theta(b_B - b_K) H_0^{(1)}(\sqrt{|B_7^2|}b_B) J_0(\sqrt{|B_7^2|}b_K) + (b_B \leftrightarrow b_K) \right] , \tag{26}$$

and

$$H_7^{(b)}(Ab_B, C_7 b_B, C_7 b_K) = K_0(Ab_B) h(C_7 b_B, C_7 b_K) , \tag{27}$$

are derived from Figs. 2(a) and 2(b), respectively. The relation $M_7^S = -M_7^P$ reflects the equality of the parity-conserving and parity-violating contributions induced by O_7.

Four diagrams, Figs. 3(a)-(d), are associated with the operator O_8, where the photon is radiated by each quark in the B or K^* mesons. The corresponding amplitudes are

$$M_8^S = -\Gamma^{(0)} \frac{1}{3} \int_0^1 dx_B dx_K \int_0^{1/\Lambda} b_B db_B b_K db_K \phi_B(x_B)\phi_{K^*}(x_K)$$
$$\times \left\{ (1 - r^2 + x_B)(r x_K + x_B) H_8^{(a)}(Ab_K, B_8 b_B, B_8 b_K) F_8(t_{8a}) \right.$$
$$+ [(2-3r)x_K - x_B + r(1-x_K)(r x_K - 2r x_B + 3x_B)]$$
$$\times H_8^{(b)}(Ab_B, C_8 b_B, C_8 b_K) F_8(t_{8b})$$
$$\left. + (1+r)(1-r^2)[(1+r)x_B - r x_K] \right.$$
$$\times H_8^{(c)}(\sqrt{|A'^2|}b_K, D_8 b_B, D_8 b_K) F_8(t_{8c})$$

$$
\begin{aligned}
&-[(1-r^2)((1-r^2)(2-x_K)+(1+3r)(2x_K-x_B))\\
&\quad +2r^2x_K(x_K-x_B)]\\
&\quad \times H_8^{(d)}(\sqrt{|A'^2|}b_B,E_8b_B,E_8b_K)F_8(t_{8d})\Big\}\,, \qquad (28)\\
M_8^P=\Gamma^{(0)}&\frac{1}{3}\int_0^1 dx_Bdx_K\int_0^{1/\Lambda} b_Bdb_Bb_Kdb_K\phi_B(x_B)\phi_{K^*}(x_K)\\
&\times\Big\{(1-r^2+x_B)(rx_K+x_B)H_8^{(a)}(Ab_K,B_8b_B,B_8b_K)F_8(t_{8a})\\
&+[(2-3r)x_K-x_B-r(1-x_K)(rx_K-2rx_B+3x_B)]\\
&\quad \times H_8^{(b)}(Ab_B,C_8b_B,C_8b_K)F_8(t_{8b})\\
&+(1-r)(1-r^2)[(1+r)x_B-rx_K]\\
&\quad \times H_8^{(c)}(\sqrt{|A'^2|}b_K,D_8b_B,D_8b_K)F(t_{8c})\\
&-[(1-r^2)((1-r^2)(2+x_K)-(1-3r)x_B)\\
&\quad -2r^2x_K(x_K-x_B)]\\
&\quad \times H_8^{(d)}(\sqrt{|A'^2|}b_B,E_8b_B,E_8b_K)F(t_{8d})\Big\}\,, \qquad (29)
\end{aligned}
$$

with

$$
\begin{aligned}
&A'^2=(1-r^2)(x_B-x_K)M_B^2\,,\quad B_8^2=(1-r^2+x_B)M_B^2\,,\\
&C_8^2=(1-x_K)M_B^2\,,\quad D_8^2=(1-r^2)x_BM_B^2\,,\quad E_8^2=(1-r^2)x_KM_B^2\,,\\
&t_{8a}=\max(A,B_8,1/b_B,1/b_K)\,,\\
&t_{8b}=\max(A,C_8,1/b_B,1/b_K)\,,\\
&t_{8c}=\max(\sqrt{|A'^2|},D_8,1/b_B,1/b_K)\,,\\
&t_{8d}=\max(\sqrt{|A'^2|},E_8,1/b_B,1/b_K)\,. \qquad (30)
\end{aligned}
$$

and the funciton F_8,

$$
F_8(t)=\alpha_s(t)c_8(t)\exp[-S(x_B,x_K,t,b_B,b_K)]\,. \qquad (31)
$$

The hard functions

$$
\begin{aligned}
&H_8^{(a)}(Ab_K,B_8b_B,B_8b_K)=H_7^{(b)}(Ab_K,B_8b_B,B_8b_K)\,,\\
&H_8^{(b)}(Ab_B,C_8b_B,C_8b_K)=K_0(Ab_B)h'(C_8b_B,C_8b_K)\\
&H_8^{(c)}(\sqrt{|A'^2|}b_K,D_8b_B,D_8b_K)=\\
&\qquad K_0(\sqrt{|A'^2|}b_K)h(D_8b_B,D_8b_K)\,,\quad A'^2\geq 0\,,\\
&\qquad i\frac{\pi}{2}H_0^{(1)}(\sqrt{|A'^2|}b_K)h(D_8b_B,D_8b_K)\,,\quad A'^2<0\,,\\
&H_8^{(d)}(\sqrt{|A'^2|}b_B,E_8b_B,E_8b_K)=\\
&\qquad K_0(\sqrt{|A'^2|}b_B)h'(E_8b_B,E_8b_K)\,,\quad A'^2\geq 0\,,\\
&\qquad i\frac{\pi}{2}H_0^{(1)}(\sqrt{|A'^2|}b_B)h'(E_8b_B,E_8b_K)\,,\quad A'^2<0 \qquad (32)
\end{aligned}
$$

are derived from Figs. 3(a)-(d), respectively. It is obvious that the above factorization formulas bear the features of Eq. (13).

The exponentials $\exp(-S)$ appearing in M_l^i are the complete Sudakov form factors with the exponent

$$S = s(x_B P_B^-, b_B) + 2\int_{1/b_B}^{t} \frac{d\mu}{\mu}\gamma_q(\alpha_s(\mu)) \\ +s(x_K P_K^+, b_K) + s((1-x_K)P_K^+, b_K) + 2\int_{1/b_K}^{t} \frac{d\mu}{\mu}\gamma_q(\alpha_s(\mu)). \tag{33}$$

The wave functions ϕ_B and ϕ_{K^*} satisfy the normalization,

$$\int_0^1 \phi_i(x)dx = \frac{f_i}{2\sqrt{6}}\,, \tag{34}$$

with the decay constant f_i, $i = B$ and K^*. The wave function for the K^* meson with transverse polarizations has been derived using QCD sum rules [12], which is given by

$$\phi_{K^*} = \frac{f_{K^*}}{\sqrt{6}}\frac{15}{4}(1-\xi^2) * [0.267(1-\xi^2)^2 + 0.017 + 0.21\xi^3 + 0.07\xi]\,, \tag{35}$$

with $\xi = 1-2x$. As to the B meson wave functions, we employ two models [21,22],

$$\phi_B^{(I)}(x) = \frac{N_B x(1-x)^2}{M_B^2 + C_B(1-x)}\,, \tag{36}$$

$$\phi_B^{(II)}(x) = N_B'\sqrt{x(1-x)}\exp\left[-\frac{1}{2}\left(\frac{xM_B}{\omega}\right)^2\right]\,, \tag{37}$$

where N_B and N_B' are normalization constants; while C_B and ω are shape parameters.

IV. RESULTS AND DISCUSSIONS

In the evaluation of the various form factors and amplitudes, we adopt $G_F = 1.16639 \times 10^{-5}$ GeV^{-2}, the flavor number $n_f = 5$, the decay constants $f_B = 200$ MeV and $f_{K^*} = 220$ MeV, the CKM matrix elements $|V_{ts}^* V_{tb}| = 0.04$, the masses $M_c = 1.5$ GeV, $M_B = 5.28$ GeV and $M_{K^*} = 0.892$ GeV, the $\bar{B}^0$ meson lifetime $\tau_{B^0} = 1.53$ ps, and the QCD scale $\Lambda = 0.2$ GeV [10]. We find that, no matter what value of the shape parameter C_B is chosen, the model $\phi_B^{(I)}$ in Eq. (36) with a flat profile leads to results smaller than the CLEO data which gives $\mathcal{B}(B \to K^*\gamma) = (4.2 \pm 0.8 \pm 0.6) \times 10^{-5}$ [3]. In fact, the maximal prediction from $\phi_B^{(I)}$, corrsponding to the shape parameter $C_B = -M_B^2$, is about 3.0×10^{-5}, close to the lower bound of the data.

On the other hand, using model $\phi_B^{(II)}$ in Eq. (37) with a sharp peak at small x, we obtain a prediction much closer to the experimental data. It is indeed found that, as $\omega = 0.795$ GeV, a prediction 4.204×10^{-5} for the branching ratio is reached, which is equal to the central value of the experimental data. If varying the shape parameter to both $\omega = 0.79$ GeV and $\omega = 0.80$ GeV, we obtain the branching ratios 4.25×10^{-5} and 4.14×10^{-5}, respectively. It indicates that the allowed range for ω is wide due to the yet large uncertainties of the data.

The detailed contribution from each amplitude M_l^i is listed in Table II in the unit of 10^{-6} GeV^{-2}. It is clear that M_7^S and M_7^P together give dominant contributions to the decay width. One also sees that M_2^S and M_2^P are smaller by an order of magnitude, while the amplitudes associated with O_8 are highly suppressed. In table II, it is interesting to note that M_2^S adds constructively to M_7^S, *i.e.*, $|M_2^S + M_7^S|^2 > |M_7^S|^2$. On the contrary, M_2^P is destructive to M_7^P. Due to this cancellating effect, the inclusion of O_2 contribution only enhances the total rate by 2% (This result is basically consistent with the estimation obtained in [13]). This result is not sensitive to the choice of ω. We obtain the same enhancement for the total rate with ω chosen to be 0.79 GeV and 0.80 GeV, respectively.

By fitting our prediction for the branching ratio $\mathcal{B}(B \to K^*\gamma)$ to the CLEO data, we determine the B meson wave function,

$$\phi_B(x) = 0.740079\sqrt{x(1-x)}\exp\left[-\frac{1}{2}\left(\frac{xM_B}{0.795\ \text{GeV}}\right)^2\right] , \tag{38}$$

which possesses a sharp peak at the low momentum fraction x. We stress that, however, Eq. (38) is not conclusive because of the large allowed range of the shape parameter ω. A more precise B meson wave function can be obtained by considering a global fit to the data of various decay modes, including $B \to D^{(*)}\pi(\rho)$ [23]. Once the B meson wave fucntion is fixed, we shall employ it in the evaluation of the nonleptonic charmless decays.

Finally, as mentioned in the Introduction, the authors of Ref. [14] found that the diagrams without hard-gluon exchanges dominate over Figs. 2(a) and 2(b) we have evaluated (only the operator O_7 was considered in the calculation of the branching ratio $\mathcal{B}(B \to K^*\gamma)$ in [14]): the latter contribute at most 23% to the branching ratio, or 12% to the decay amplitude. However, in that analysis, α_s is set to 0.2, which is even smaller than $\alpha_s(M_B) = 0.23$ evaluated at the B meson mass. We argue that such a small coupling constant is inappropriate, since the momentum flow involved in the decay process is most likely less than the b quark mass M_b, say, roughly $1 \sim 2$ GeV, which corresponds to $\alpha_s \approx 0.4$. The K^* meson mass was neglected in [14], such that Fig. 2(a) does not contribute. In our analysis we did not make this approximation, and observed that the contribution from Fig. 2(a) is about $M_{K^*}/M_B \approx 1/5$ of that from Fig. 2(b). Moreover, a flat B meson wave function corresponding to the shape parameter $\omega \approx 1.3$ GeV was adopted in the computation of the higher-order contributions in [14], which is far beyond $\omega \approx 0.4$ GeV specified in [22]. If a sharper B meson wave function is employed, these contributions will be enhanced at least by a factor of 3. Note that the leading-order contributions considered in [14] are less sensitive to the variation of ω in the wave function. Adding up the above enhancements, the amplitude for $O(\alpha_s)$-corrections becomes approximately equal to the leading-order contribution. In this sense the analysis in [14] does not seem to be self-consistent.

In our approach, the momentum of the spectator quark in the B meson is parametrized into the minus direction, while the momentum of the spectator quark in the K^* meson is parametrized in the plus direction. This parametrization is appropriate because of the hard gluon exchange. Note that the factorization formulas presented in Sect. III are constructed based on the diagrams with at least one hard gluon exchange. For example, the infrared divergences from self-energy corrections to the spectator quark are factorized into the B meson wave function, if they occur before the hard gluon exchange; and into the K^* meson wave function, if they occur after the hard gluon exchange. Without hard gluons to distinguish the initial and final states, factorization of self-energy corrections to the spectator

quark is ambiguous. Therefore, the diagrams without hard gluons do not appear in the regime of PQCD factorization theorems, and those with one hard gluon are indeed leading. If ignoring the validity of the factorization, we may proceed with evaluating the contribution of O_7 from the diagram without hard gluons in the PQCD framework. It is trivial to obtain the hard subamplitude in momentum space,

$$H_7^{(0)} = \frac{(1+r)(1-r^2)}{2M_B}\delta^3(k_1-k_2)\;, \tag{39}$$

where the δ-function requires that the longitudinal momenta of the spectrator quarks in the B and K^* mesons are in the same direction. Fourier transforming the above expression into b space, and convoluting it with the wave funcitons in Eqs. (35) and (38) and with the Sudakov factor, we derive the amplitudes

$$\begin{aligned} M_7^{S(0)} = -M_7^{P(0)} = \Gamma^{(0)}\int_0^1 dx\int_0^{1/\Lambda} bdb\phi_B(x)\phi_{K^*}(x) \\ \times\frac{(1+r)(1-r^2)}{4\pi^2 M_B^2 C_F}c_7(1/b)\exp[-S(x,x,1/b,b,b)]\;. \end{aligned} \tag{40}$$

Without hard gluons, the momentum fraction x and the transverse extent b are equal for the B and K^* mesons. We have set the hard scale t to $1/b$ due to the lack of gluon momentum transfer. A simple numerical work on Eq. (40) gives $M_7^{S(0)}/\Gamma^{(0)} = -2.51\times 10^{-6}$ GeV^{-2}, which is of the same order as the contributions from O_2 and O_8. One of the reasons for the smallness of $M_7^{S(0)}$, compared to the values obtained in [14], is the additional strong Sudakov suppression. Referred to M_7^S listed in Table II, $M_7^{S(0)}$ is negligible. If including $M_7^{S(0)}$ and $M_7^{P(0)}$, the branching ratio $B(B\to K^*\gamma)$ will increase by only 1.7%.

V. CONCLUSION

In this paper we have extended the PQCD three-scale factorization theorem to the penguin-induced radiative decay $B\to K^*\gamma$, which takes into account the Sudakov resummation for large logarithmic corrections to this process. We have included the non-spectator contribution from the current-current operator O_2 besides the standard contribution given by magnetic-penguin operators O_7 and O_8. It turns out that the contribution by O_2 is negligible due to certain cancellations. The contributions from O_8 and other operators in the effective Hamiltonian are also quite small. Finally, we have determined the B meson wave function from the best fit to the experimental data of $\mathcal{B}(B\to K^*\gamma)$, which will be employed to make predictions of other B meson decays.

ACKNOWLEDGMENTS

We thank X.-G. He and W.-S. Hou for discussions. This work was supported in part by the National Science Council of R.O.C. under the Grant Nos. NSC-88-2112-M-006-013 and NSC-88-2112-M-009-002.

REFERENCES

[1] R. Ammar *et al.* (CLEO Collaboration), Phys. Rev. Lett. **71**, 674 (1993).

[2] M. S. Alam *et al.* (CLEO Collaboration), Phys. Rev. Lett. **74**, 2885 (1995).

[3] R. Ammar *et al.* (CLEO Collaboration), "*Radiative Penguin Decays of the B Meson*," CONF 96-5, ICHEP-96 PA05-9 (1996).

[4] S. Glenn *et al.* (CLEO collaboration), "*Improved Measurement of* $B(b \to s\gamma)$," submitted to XXIX Int. Conf. on High Energy Physics, Vancouver, Canada, July 23-29, 1998.

[5] B. Barate *et. al* (ALEPH), "*A Measurement of the Inclusive* $b \to s\gamma$ *Branching Ratio*," CERN-EP/98-044 (1998).

[6] A. Falk, M. Luke and M. Savage, Phys. Rev. D **49**, 3367 (1994).

[7] H-n. Li and H.L. Yu, Phys. Rev. Lett. **74**, 4388 (1995); Phys. Lett. B **353**, 301 (1995); Phys. Rev. D **53**, 2480 (1996).

[8] H-n. Li, Phys. Rev. D **52**, 3958 (1995).

[9] H-n. Li and H.L. Yu, Phys. Rev. D **53**, 4970 (1996).

[10] C.H. Chang and H-n. Li, Phys. Rev. D **55**, 5577 (1997); T.W. Yeh and H-n. Li, Phys. Rev. D **56**, 1615 (1997).

[11] V.L. Chernyak and A.R. Zhitnitsky, Phys. Rep. **112**, 173 (1984).

[12] M. Benayoun and V.L. Chernyak, Nucl. Phys. **B 329**, 285 (1990).

[13] J. Milana, Phys. Rev. D **53**, 1403 (1996).

[14] C. Greub, H. Simma and D. Wyler, Nucl. Phys. **B 434**, 39 (1995).

[15] For a review on earlier literatures, see G. Buchalla, A. J. Buras and M. E. Lautenbacher, Review of Modern Physics, **68**, 1125 (1996).

[16] The signs of O_7 and O_8 are consistent with the covariant derivative $D_\mu = \partial_\mu + igT^a A^a_\mu + ieQA_\mu$, where A^a_μ and A_μ denote gluon and photon fields respectively.

[17] Strictly speaking, the order of this diagram is $eG_F(A_1\alpha_s \ln\frac{M_W}{\mu} + B_1\alpha_s + A_2\alpha_s^2 \ln^2\frac{M_W}{\mu} + B_2\alpha_s^2 \ln\frac{M_W}{\mu} + \cdots)$, where coefficients A_i and B_i represent contributions from leading and next-to-leading logarithms. We simply count the order according to the first two terms in the series, $A_1\alpha_s \ln\frac{M_W}{\mu}$ and $B_1\alpha_s$. Same rule of counting applies to diagrams in Fig. 1-3.

[18] H.-Y. Cheng, C.-Y. Cheung, G.-L. Lin, Y.-C. Lin, T.-M. Yan and H.-L. Yu, Phys. Rev. **D 51**, 1199 (1995).

[19] J. Liu and Y.-P. Yao, Phys. Rev. **D 42**, 1485 (1990).

[20] The off-shell $b \to sg^*\gamma$ vertex was also calculated by Simma and Wyler in Nucl. Phys. **B 344**, 283 (1990); and by Milana in Ref. [13]. Here we follow the convention of Ref. [19].

[21] F. Schlumpf, Report No. hep-ph/9211255; R. Akhoury, G. Sterman and Y.-P Yao, Phys. Rev. D **50**, 358 (1994).

[22] M. Bauer and M. Wirbel, Z. Phys. C **42**, 671 (1989).

[23] H-n. Li and B. Melic, e-print hep-ph/9902205.

FIGURES

FIG. 1. Contributions to the $B \to K^*\gamma$ decay from the current-current operator O_2. The diagram with a photon emitted from the other side of the charm-quark loop is not shown.

FIG. 2. Contributions to the $B \to K^*\gamma$ decay from the magnetic-penguin operator O_7.

FIG. 3. Contributions to the $B \to K^*\gamma$ decay from the chromo-magnetic-penguin operator O_8.

FIG. 4. Contributions to the $B \to K^*\gamma$ decay from the strong-penguin operators $O_3, O_4, \cdots O_6$. The dark square denotes insertions of the operators $O_3, O_4, \cdots O_6$.

FIG. 5. Contributions to the $B \to K^*\gamma$ decay from an O_2-insertion and a *bremsstrahlung* photon.

Table I. Hard subamplitudes obtained from Figs. 1-3. The quantities $\tilde{A}_4$ and $\tilde{A}_5$ are integrands of I_{11} and $I_{20} - I_{10}$ respectively, where the general integral I_{ab} is defined in Eq. (10).

Diagram	H^S
O_2	$\frac{4}{3}\frac{(1-r)(1-r^2)x_K[(1-r^2+2rx_K+2x_B)\tilde{A}_4+(rx_K+3x_B)\tilde{A}_5]}{x_Kx_Bm_B^2+(\mathbf{k}_{KT}-\mathbf{k}_{BT})^2}$
$O_7(a)$	$\frac{2r(1-r^2)}{[x_Kx_Bm_B^2+(\mathbf{k}_{KT}-\mathbf{k}_{BT})^2][(x_B-r)m_B^2+k_{BT}^2]}$
$O_7(b)$	$\frac{2(1-r^2)[1+r+(1-2r)x_K]}{[x_Kx_Bm_B^2+(\mathbf{k}_{KT}-\mathbf{k}_{BT})^2](x_Km_B^2+k_{KT}^2)}$
$O_8(a)$	$-\frac{(1-r^2+x_B)(rx_K+x_B)}{3[x_Kx_Bm_B^2+(\mathbf{k}_{KT}-\mathbf{k}_{BT})^2][(1-r^2+x_B)m_B^2+k_{BT}^2]}$
$O_8(b)$	$-\frac{(2-3r)x_K-x_B+r(1-x_K)(rx_K-2rx_B+3x_B)}{3[x_Kx_Bm_B^2+(\mathbf{k}_{KT}-\mathbf{k}_{BT})^2][(x_K-1)m_B^2+k_{KT}^2]}$
$O_8(c)$	$-\frac{(1+r)(1-r^2)[(1+r)x_B-rx_K]}{3[(1-r^2)(x_B-x_K)m_B^2+(\mathbf{k}_{KT}-\mathbf{k}_{BT})^2][(1-r^2)x_Bm_B^2+k_{BT}^2]}$
$O_8(d)$	$\frac{(1-r^2)[(1-r^2)(2-x_K)+(1+3r)(2x_K-x_B)]+2r^2x_K(x_K-x_B)}{3[(1-r^2)(x_B-x_K)M_B^2+(\mathbf{k}_{KT}-\mathbf{k}_{BT})^2][(r^2-1)x_Km_B^2+k_{KT}^2]}$

Diagram	H^P
O_2	$\frac{4}{3}\frac{(1-r^2)x_K[(1-r)(1-r^2)+2r^2x_K+2x_B)\tilde{A}_4+(r(1+r)x_K+(3-rx_B))\tilde{A}_5]}{x_Kx_Bm_B^2+(\mathbf{k}_{KT}-\mathbf{k}_{BT})^2}$
$O_7(a)$	$-\frac{2r(1-r^2)}{[x_Kx_Bm_B^2+(\mathbf{k}_{KT}-\mathbf{k}_{BT})^2][(x_B-r)m_B^2+k_{BT}^2]}$
$O_7(b)$	$-\frac{2(1-r^2)[1+r+(1-2r)x_K]}{[x_Kx_Bm_B^2+(\mathbf{k}_{KT}-\mathbf{k}_{BT})^2](x_Km_B^2+k_{KT}^2)}$
$O_8(a)$	$\frac{(1-r^2+x_B)(rx_K+x_B)}{3[x_Kx_Bm_B^2+(\mathbf{k}_{KT}-\mathbf{k}_{BT})^2][(1-r^2+x_B)m_B^2+k_{BT}^2]}$
$O_8(b)$	$\frac{(2-3r)x_K-x_B-r(1-x_K)(rx_K-2rx_B+3x_B)}{3[x_Kx_Bm_B^2+(\mathbf{k}_{KT}-\mathbf{k}_{BT})^2][(x_K-1)m_B^2+k_{KT}^2]}$
$O_8(c)$	$\frac{(1-r)(1-r^2)[(1+r)x_B-rx_K]}{3[(1-r^2)(x_B-x_K)m_B^2+(\mathbf{k}_{KT}-\mathbf{k}_{BT})^2][(1-r^2)x_Bm_B^2+k_{BT}^2]}$
$O_8(d)$	$-\frac{(1-r^2)[(1-r^2)(2+x_K)-(1-3r)x_B]-2r^2x_K(x_K-x_B)}{3[(1-r^2)(x_B-x_K)M_B^2+(\mathbf{k}_{KT}-\mathbf{k}_{BT})^2][(r^2-1)x_Km_B^2+k_{KT}^2]}$

Table II. The amplitudes M_l^i in the unit of 10^{-6} GeV^{-2}.

M_2^S/Γ_0	M_7^S/Γ_0	M_8^S/Γ_0
$-2.46-14.17i$	$-140.14-143.31i$	$-0.58+1.10i$
M_2^P/Γ_0	M_7^P/Γ_0	M_8^P/Γ_0
$-1.21-11.05i$	$140.14+143.31i$	$0.54-1.33i$

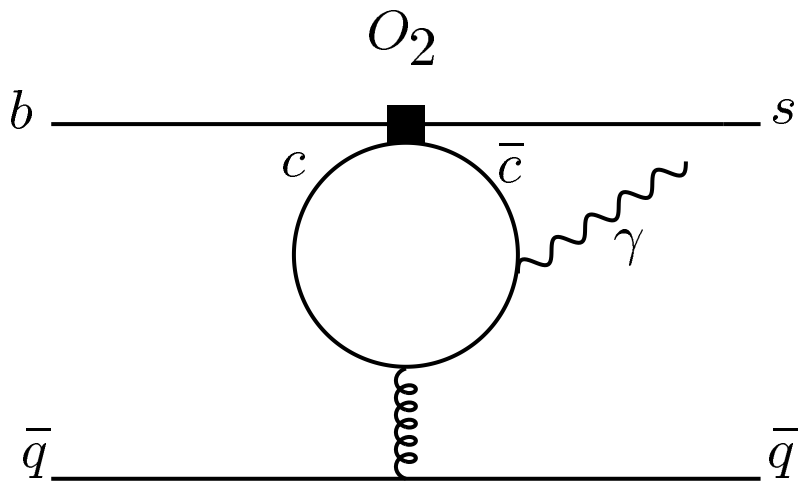

Fig. 1

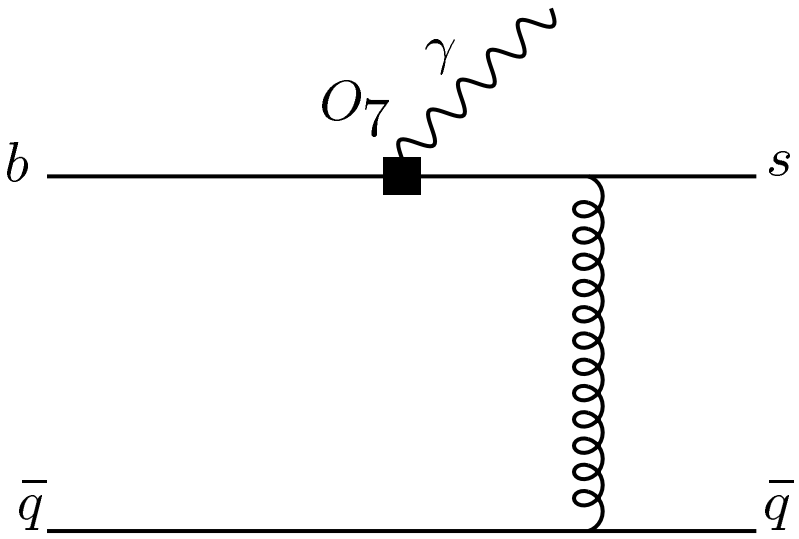

(a)

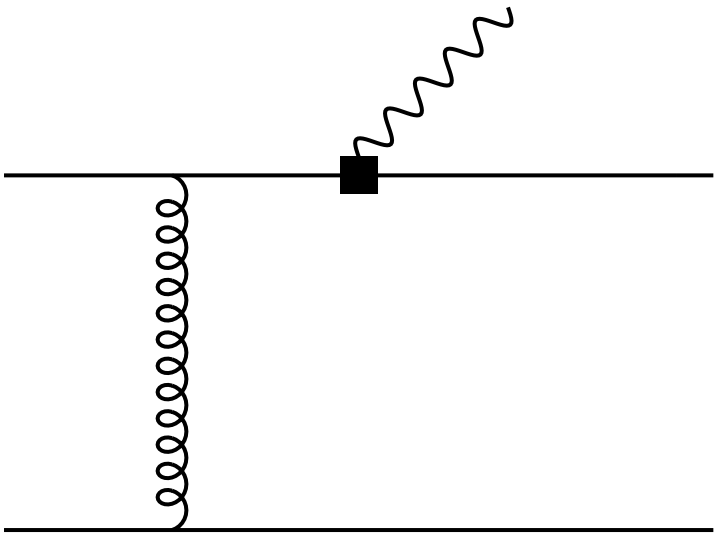

(b)

Fig. 2

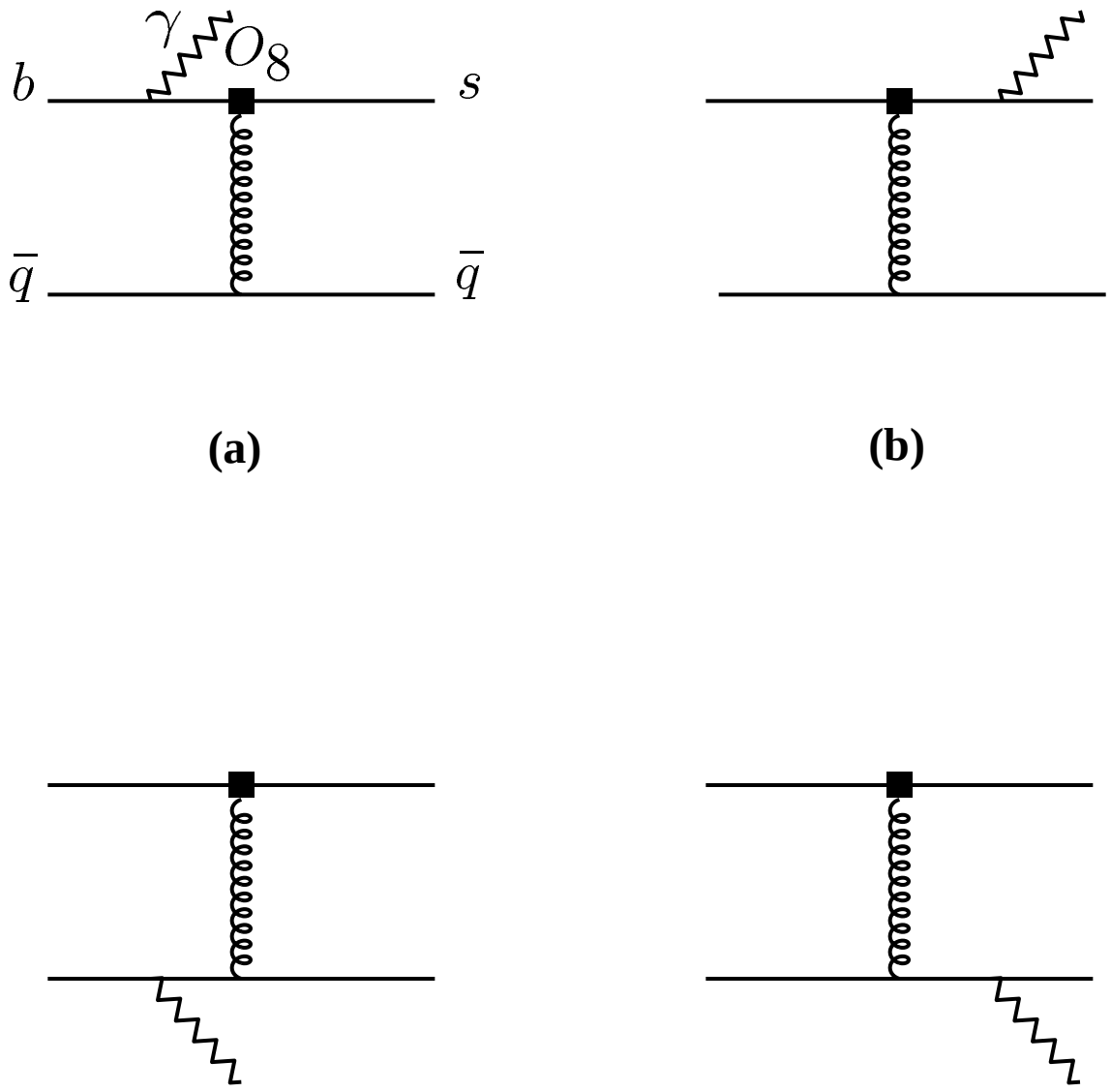

Fig. 3

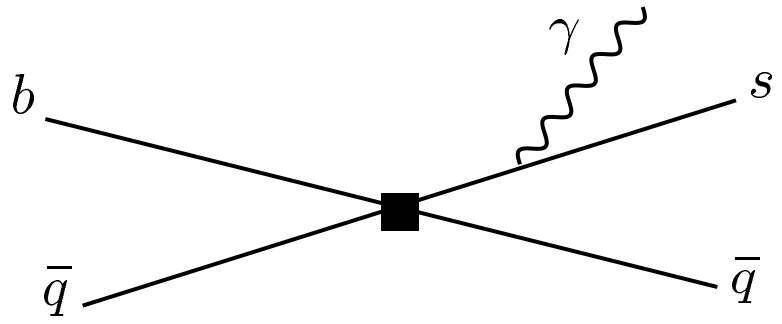

Fig. 4

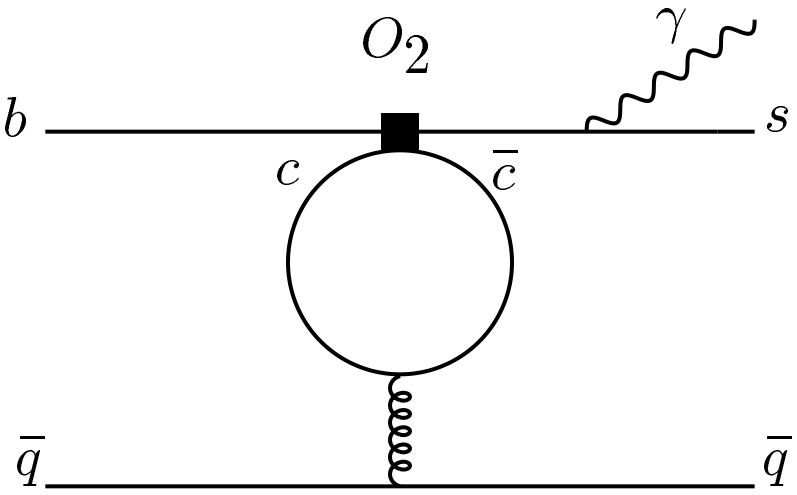

Fig. 5